Scripta Materialia 163 (2019) 66–70

Contents lists available at ScienceDirect

Scripta Materialia

journal homepage: www.elsevier.com/locate/scriptamat

# Mechanisms of grain boundary migration and growth in nanocrystalline metals under irradiation

Miaomiao Jin, Penghui Cao*, Michael P. Short

*Department of Nuclear Science and Engineering, Massachusetts Institute of Technology, Cambridge, Massachusetts 02139, United States of America*
*Department of Mechanical and Aerospace Engineering, University of California, Irvine, Irvine, California 92697, United States of America*

ARTICLE INFO

*Article history:*
Received 24 October 2018
Received in revised form 21 December 2018
Accepted 28 December 2018
Available online xxxx

*Keywords:*
Nanocrystalline
Grain boundary migration
Grain growth
Radiation
Molecular dynamics

ABSTRACT

Atomistic simulations of radiation damage uncover how grain boundaries (GBs) migrate and coalesce under irradiation in bicrystalline Cu. Planar GB migration biased by defect cluster-mediated attraction first leads to slow and steady motion. Subsequently, adjoining GBs coalesce into curved surfaces, where curvature-driven migration with a velocity three orders of magnitude higher than that of a planar boundary dominates motion, triggering rapid grain growth. This study reveals the atomistic mechanisms of radiation-induced grain growth, and has practical implications towards engineering radiation-tolerant nanostructures.



Internal interfaces such as grain boundaries (GBs) play a central role in governing many material properties in metals. For example, decreasing grain size to the nanometer scale, which increases the volume density of GBs, considerably improves mechanical strength [1]. Microstructural evolution due to grain growth is controlled by a key process - GB migration. The growth of one grain at the expense of others can be driven by various forces, from elastic energy anisotropy, non-uniform defect or impurity density, a gradient in temperature, and capillary forces of curved GBs [2]. These driving forces are frequently considered in experiments and simulations to study GB migration and grain growth in a variety of polycrystalline systems [3-5].

Boundaries and interfaces act as effective radiation damage sinks by rapidly absorbing radiation-induced defects [6]. To this extent, nanocrystalline metals with a high volume density of boundaries are promising radiation-tolerant structural materials, but they inevitably experience radiation-enhanced GB motion and growth [7,8] accompanied by mechanical property degradation. In studies of irradiated polycrystalline metals, the average grain size increases with irradiation dose with a power law relationship depending on microstructural characteristics and irradiation conditions [9,10]. Theoretical models based on thermal spikes were proposed to interpret the nature of radiation-induced grain growth [11,12], in which a GB is hypothesized to migrate through biased atomic diffusion. The process is assumed to occur within the displacement cascade (i.e. thermal spike) region in the vicinity of the GB, and is driven by local curvature. This radiation-induced GB motion has also been observed in MD simulations of displacement cascades in nanocrystalline metals, but only arises if the thermal spike exceeds the grain size and overlaps the boundaries [13]. Although the aforementioned experiments and simulations of polycrystalline materials construct a picture of the overall change in grain size, it is difficult to extract a clear understanding of precisely how GBs respond to radiation damage, due to the complexity of microstructures which encompass connected GBs and limitations in temporal and spatial resolution of experiments.

A bicrystal system is a reasonable alternative to investigate individual boundaries. To induce GB motion, external forces are typically applied to the system, including shear stress [14], elastic stored energy [15], vacancy loading [16] and artificial synthetic forces [17], which have been considered in both experiments and simulations. The resultant GB migration rates were found to be proportional to the magnitude of each force. Without external forces or internal energy gradients, planar GBs generally exhibit random-walk migration [18]. How they evolve under irradiation is an open and interesting scientific question, which is also of central importance to understanding radiation-induced grain growth.

* Corresponding author.
*E-mail address:* caoph@uci.edu (P. Cao).

https://doi.org/10.1016/j.scriptamat.2018.12.038
1359-6462/ 

Here, we examine a high-angle planar GB's response to radiation damage through a series of consecutive displacement cascade MD simulations [19]. A Cu bicrystal as shown in Fig. 1 (a) is constructed, containing two symmetrical tilt, high-angle Σ5(210) GBs with dimensions of 2λ × 11.4 nm × 10.9 nm, where λ (taken here as 11.4 nm) represents the spacing between adjacent GBs. We model Cu-Cu interactions using an embedded-atom method (EAM) potential [20] which is smoothly joined [21] to a Ziegler-Biersack-Littmark (ZBL) repulsive potential to resolve highly energetic collisions [22,23]. The system is first equilibrated to zero pressure for 100 ps at 800 K with periodic boundary conditions, followed by damage cascade simulations using the same procedure as described in [24]. Specifically, a cascade is modeled by assigning a kinetic energy of 5 keV with an arbitrary direction to a randomly selected primary knock-on atom (PKA) and annealing for 30,000 adaptive timesteps, with a thermal sink at the boundaries to cool the system to ~800 K after the cascade. This process is repeated up to experimental radiation dose levels by successively introducing 2000 cascades with randomly chosen PKAs, achieving a dose level of ~1.42 dpa according to the NRT [25] approximation in a total simulation time of 58 ns. It should be noted that this procedure inevitably leads to a much higher dose rate compared with experiments. Nevertheless, it provides a representative view of microstrutural evolution driven by collision cascades. The simulations were performed using the large-scale atomic and molecular massively parallel simulator (LAMMPS) [26], and the simulation data repository is available at [27] with the input and output files, and processing scripts used in the creation of this manuscript.

Fig. 1 (a) depicts the simulation model with two GBs located at $X = -5.7$ and 5.7 nm, respectively. During collision cascades, GB positions are recorded and plotted as a function of time as shown in Fig. 1 (b). GBs are observed to move towards each other under the applied, constant radiation flux. A close inspection of the position-time plots reveals two pronounced characteristics: GB motion exhibits a temporally intermittent manner, manifested by abrupt position changes interspersed in the curves, and a back-and-forth motion is superimposed on a general trend of GBs approaching each other. Such features reflect volatile GB behavior under the combined influence of collision cascades, thermally-activated diffusion, and defect-GB interactions. The two GBs move at about the same velocity $V \sim 0.08$ m/s to the center of simulation box, followed by direct interaction with each other, leading to final grain growth which will be elaborated below. Correspondingly, the system potential energy (energy of inherent structure [28]) exhibits a drastic drop as shown in Fig. 1 (c), indicating energy release accompanied by GB annihilation. Fig. 1 (c) also shows that the system energy gradually builds up at the beginning of irradiation, owing to the extra energy introduced by radiation defects into the originally perfect crystal. After ~3 ns, the defect concentration reaches saturation where defect creation and annihilation strike a balance, giving rise to a roughly constant system energy before the drop associated with grain growth. It is worth noting that in Fig. 2 (b) the two GBs preferentially migrate to the center, but our ten independent simulations indicate that GBs are equally likely to move outwards, interacting at the system boundary. Due to the periodic boundary conditions, there is no difference between motion in one direction or the other.

We then focus on the detailed microstructural evolution of the system, particularly on atomistic processes of boundary evolution and grain growth resulting from GB migration. In Fig. 2, we show the microstructural evolution of the system before, during, and after grain growth at times from 43.12 to 54.42 ns. At 43.12 ns, the GBs have considerably shifted away from their original locations and approach each other (Fig. 2 (a)). The boundary profiles become wider and rougher as they preferentially absorb radiation-induced interstitials. In the bulk region, vacancy clusters rearrange to more energetically favorable stacking fault tetrahedra (SFTs). Attraction due to the elastic interaction [24] between SFTs and irradiated (interstitial-loaded) GBs provides the necessary driving force for GB migration. The SFTs in the reduced bulk region are synergistically absorbed by the moving GBs (refer to the supplementary video) which results in a defect-scarce zone. At 54.28 ns as shown in Fig. 2 (b), the boundaries simultaneously interact with the same defect. With the small separation distance ~4 nm, the elastic interaction between the two GBs could increase the driving force for attraction. Subsequently, the two GBs have come into direct contact (Fig. 2 (c)), leaving a small region of perfect atomic structure where the GBs are partially annihilated. From this point, the two planar boundaries transform into a curved surface, and the migration becomes curvature-driven with a

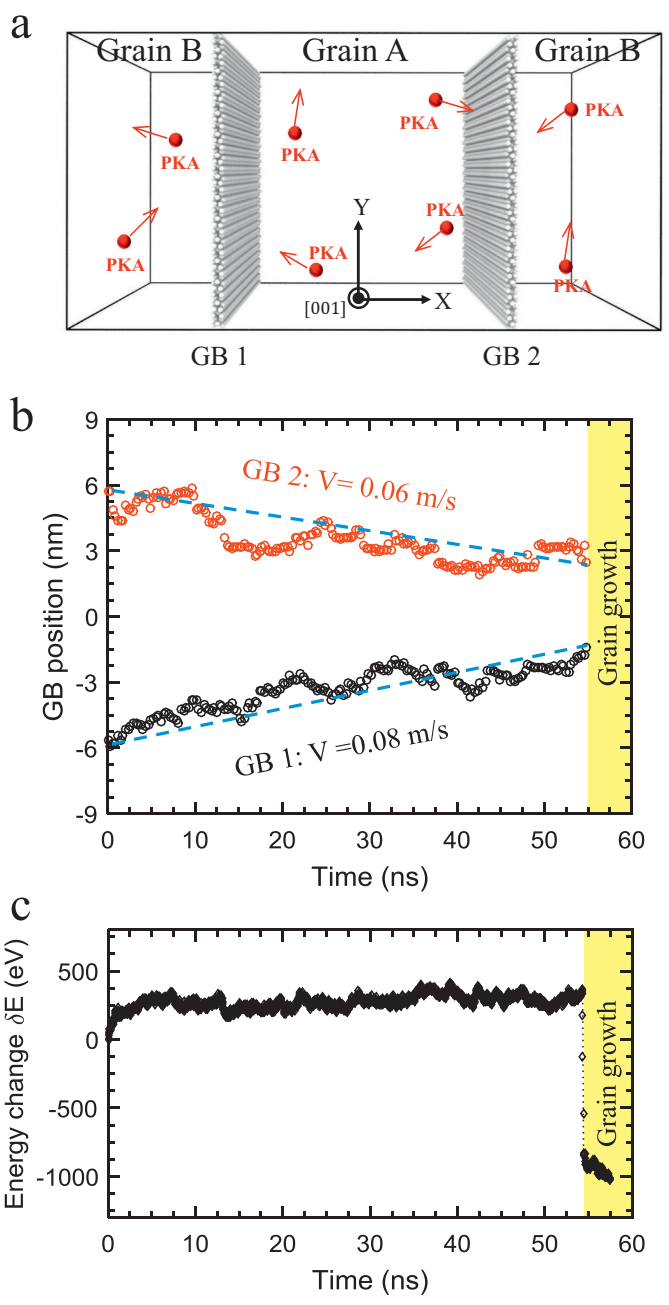


**Fig. 1.** (a) Illustrates the bicrystal model with two Σ5(210) boundaries. Primary knock-on atoms (PKAs) are randomly selected and homogeneously distributed in the system. (b) shows GB position as a function of time during irradiation at 800 K, where the slope represents GB velocity. (c) shows the corresponding system energy change $\delta E$ with time.

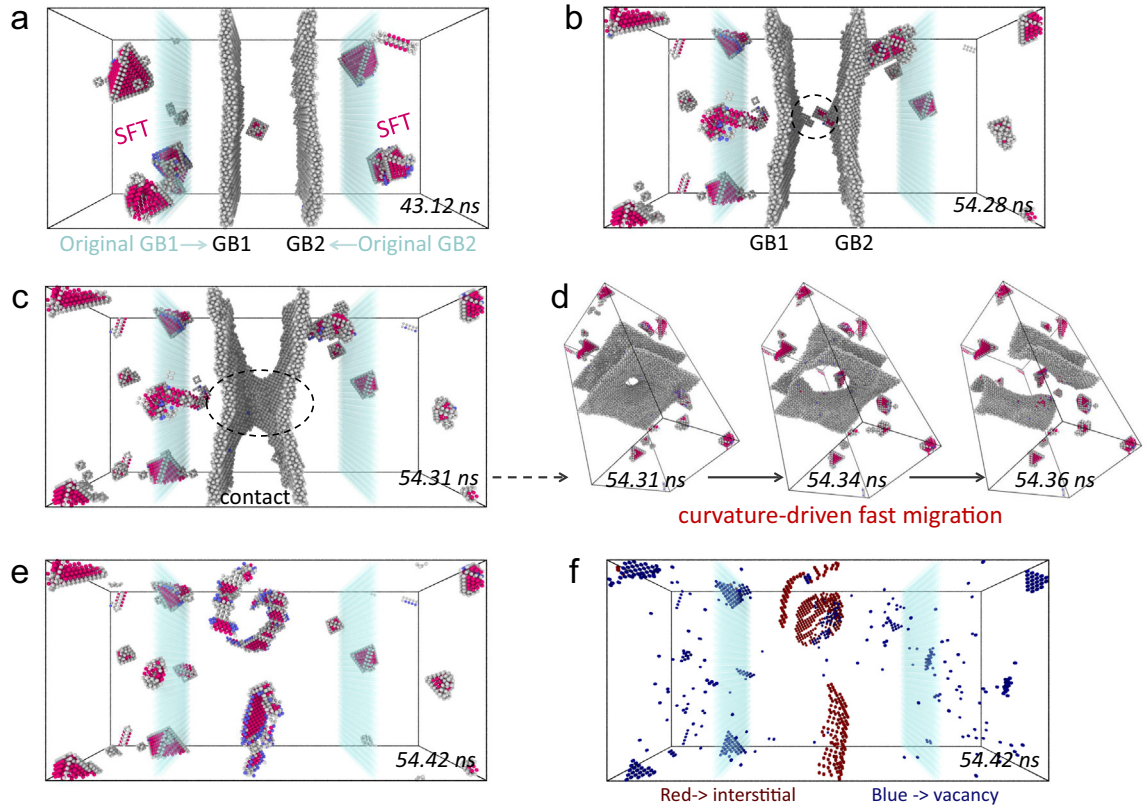


**Fig. 2.** Microstructural evolution of a Cu bicrystal under irradiation at 800 K. (a) Structures of irradiated GBs and SFTs at 43.12 ns; (b) two GBs simultaneously interacting with a defect at 54.8 ns; (c) GBs connecting at 54.21 ns and curvature-driven migration leading to GB annihilation (d); (e) defect distribution following GB annihilation at 54.42 ns, and corresponding interstitial and vacancy type structures shown in (f). Atoms are colored by structure, and the shaded turquoise indicates the initial GB location. Only large atom clusters are shown in (a–e) for ease of visualization.

significantly increased velocity of ~102 m/s (see Fig. 2 (d)). Comparing to the planar boundary velocity of ~0.08 m/s, the speed of the curved one increases by three orders of magnitude, signifying the effects of curvature on GB migration. One can also see in Fig. 2 (d) that the boundary (hole) migration is anisotropic, due to orientation-dependent boundary stiffness and the formation of minimum free energy surfaces. In Fig. 2 (e), planar stacking faults are left behind after GB annihilation, formed by the collapse of interstitials on the close-packed {111} planes terminated by partial dislocations. Corresponding to the same atomic structure as in Fig. 2 (e), Fig. 2 (f) shows the distribution of interstitial and vacancy defects analyzed by Wigner-Seitz cell method [23].

During irradiation, GBs preferentially absorb interstitials to become interstitial-loaded, and these irradiated boundaries can differ from the pristine ones in terms of mobility. The boundary velocity $V$ could be described with the product of a driving force $P$ and the intrinsic mobility $M$. However, the intractability of the driving force in the irradiation condition renders the calculation of mobility impractical. To characterize the migration properties of irradiated (interstitial-loaded) and pristine GBs, we adopt the continuum model [18] to extract GB mobility in the limit of zero driving force. We perform additional 30 independent MD simulations (without cascades) for systems containing perfect or irradiated boundaries. Due to slow GB diffusion, a higher temperature of 1200 K is chosen to obtain a reliable relation between mean squared displacements (MSDs) and time, and therefore their diffusivities. Fig. 3 shows the MSD of GB position ($\langle \bar{X}^2 \rangle$) as a function of time $t$, and the linear slope represents the GB diffusion coefficient $D$. We therefore compute the mobility from a theoretical model, which relates the mobility to the diffusion coefficient by $M = DA/2k_BT$, where $A$ is the boundary plane area and $T$ is the system temperature in Kelvin. The pristine GB has a mobility $M = 1.6 \times 10^{-8} m^4 J^{-1} s^{-1}$ which is consistent with experiments [29]. The irradiated GB is far more mobile ($M = 2.2 \times 10^{-7} m^4 J^{-1} s^{-1}$),

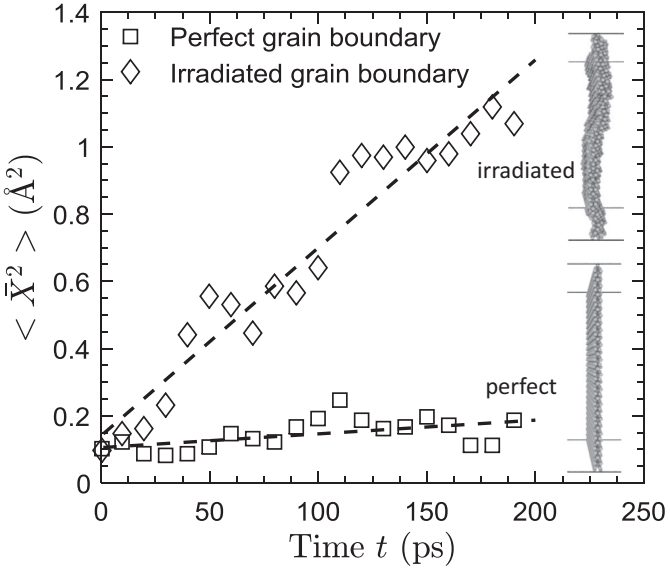


**Fig. 3.** Mean squared displacement of GBs $\langle \bar{X}^2 \rangle$ as a function of time for perfect and irradiated (interstitial-loaded) Σ5(210) boundaries at 1200 K. The boundary diffusion coefficient $D$ is the slope of a linear fit to the points in the random walk model.

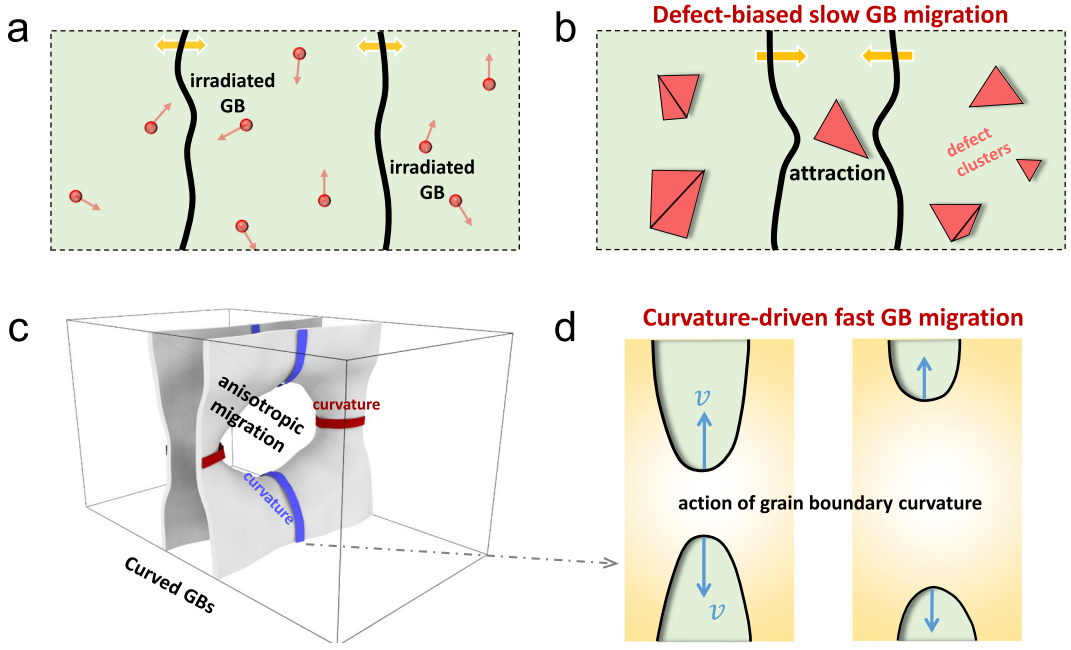


**Fig. 4.** Schematic illustration of different stages leading to grain growth under irradiation. (a) Stage I: GBs are irradiated, exhibiting random walk behavior with high mobility; (b) Stage II: defect-biased planar GB migration dominates due to synergistic attraction of defects; (c–d) Stage III: rapid curvature-driven GB migration.

possibly due to more frequent atom rearrangement and migration associated with the disordered boundary structure.

Fig. 4 illustrates a mechanistic process for radiation-induced grain growth in three stages. In the early stage of radiation damage, the GBs become interstitial-loaded, gaining a higher mobility than pristine ones. At this stage the boundaries exhibit random walk oscillations (Fig. 4 (a)). With increasing radiation dose, energetically favorable SFTs between the GBs induce attraction to further reduce interboundary distance. The boundary migration mechanism changes from random walk to biased-motion, and GBs slowly and steadily drift from their original positions. In this second stage (Fig. 4 (b)), GB drift shrinks the boundary distance to the extent that both can synergistically contribute to the capture of defects inside the smaller bulk region. When the GBs reach a small interval ($< 4$ nm in this case), they can directly interact and then connect, leading to stage III where curvature-driven boundary migration dominates (Fig. 4 (c–d)). Because the grain boundary energy is orientation-dependent, its migration is an anisotropic process as shown in Fig. 4 (c). The migration rate is significantly accelerated, owing to the high driving force from the curved-boundary. After a short duration of tens of picoseconds, the completion of migration results in GB annihilation and grain growth.

In summary, our results reveal the detailed microstructural processes underpinning grain growth in nanocrystalline Cu under irradiation. Grain boundary evolution proceeds in stages, marked by different migration mechanisms. With a gradually increasing damage level, the motion of the planar GBs starts as a random walk, and then becomes biased due to defect cluster attraction, steadily reducing GB distance. Ultimately, curvature-driven migration dominates and leads to rapid GB annihilation, with a velocity three orders of magnitude higher than that of planar boundaries. The proposed three stage mechanism of grain growth can be utilized to develop a thorough theoretical analysis of radiation-induced grain growth in polycrystalline metals when subjected to elevated temperature [30] or radiation flux [31]. The results have practical implications in engineering stable GB structures to maintain radiation resistance, and motivate further investigation into the mechanisms of grain growth in more complex systems such as polycrystalline metals.

Supplementary data to this article can be found online at https://doi.org/10.1016/j.scriptamat.2018.12.038.

## Acknowledgments

The authors acknowledge generous financial support from the U.S. Department of Energy's (DOE) Nuclear Energy University Program (NEUP) under Grant No. DE-NE0008754, and the Idaho National Laboratory (INL) Nuclear University Consortium (NUC), under the Laboratory Directed Research and Development (LDRD) Grant No. 10-112583. This research made use of the resources of the High Performance Computing Center at INL, which is supported by the Office of Nuclear Energy of the U.S. DOE and the Nuclear Science User Facilities under Contract No. DE-AC07-05ID14517.

## References

[1] N. Petch, J. Iron Steel Inst. 174 (1953) 25–28.
[2] G. Gottstein, L.S. Shvindlerman, Grain boundary migration in metals: thermodynamics, kinetics, applications, CRC press. 2009.
[3] T. Rupert, D. Gianola, Y. Gan, K. Hemker, Science 326 (2009) 1686–1690.
[4] H. Zhang, M. Upmanyu, D. Srolovitz, Acta Mater. 53 (2005) 79–86.
[5] M. Tonks, P. Millett, W. Cai, D. Wolf, Scr. Mater. 63 (2010) 1049–1052.
[6] I. Beyerlein, A. Caro, M. Demkowicz, N. Mara, A. Misra, B. Uberuaga, Mater. Today 16 (2013) 443–449.
[7] K. Yu, D. Bufford, F. Khatkhatay, H. Wang, M. Kirk, X. Zhang, Scr. Mater. 69 (2013) 385–388.
[8] L. Wu, W. Yu, S. Hu, S. Shen, J. Nucl. Mater. 505 (2018) 183–192.
[9] J.C. Liu, M. Nastasi, J. Mayer, J. Appl. Phys. 62 (1987) 423–428.
[10] J.C. Liu, J. Mayer, Nucl. Inst. Methods Phys. Res. B 19 (1987) 538–542.
[11] D.E. Alexander, G.S. Was, Phys. Rev. B 47 (1993) 2983.
[12] D. Kaoumi, A. Motta, R. Birtcher, J. Appl. Phys. 104 (2008) 073525.
[13] W. Voegeli, K. Albe, H. Hahn, Nucl. Instrum. Meth. Phys. Res. B 202 (2003) 230–235.
[14] J.W. Cahn, Y. Mishin, A. Suzuki, Coupling grain boundary motion to shear deformation, Acta Mater. 54 (2006) 4953–4975.
[15] H. Zhang, M. Mendelev, D. Srolovitz, Acta Mater. 52 (2004) 2569–2576.
[16] W. Yu, M. Demkowicz, J. Mater. Sci. 50 (2015) 4047–4065.

[17] D.L. Olmsted, E.A. Holm, S.M. Foiles, Acta Mater. 57 (2009) 3704–3713.
[18] Z.T. Trautt, M. Upmanyu, A. Karma, Science 314 (2006) 632–635.
[19] M. Jin, P. Cao, M.P. Short, Acta Mater. 147 (2018) 16–23.
[20] Y. Mishin, M. Mehl, D. Papaconstantopoulos, A. Voter, J. Kress, Phys. Rev. B 63 (2001) 224106.
[21] X.-M. Bai, A.F. Voter, R.G. Hoagland, M. Nastasi, B.P. Uberuaga, Science 327 (2010) 1631–1634.
[22] J.F. Ziegler, J.P. Biersack, U. Littmark, The Stopping and Range of Ions in Solids, Pergamon Press. 1985.
[23] K. Nordlund, M. Ghaly, R. Averback, M. Caturla, T.D. de La Rubia, J. Tarus, Phys. Rev. B 57 (1998) 7556.
[24] M. Jin, P. Cao, S. Yip, M.P. Short, Acta Mater. 155 (2018) 410–417.
[25] M. Norgett, M. Robinson, I. Torrens, Nucl. Eng. Des. 33 (1975) 50–54.
[26] S. Plimpton, P. Crozier, A. Thompson, Sandia National Laboratories 18 (2007)
[27] M.M. Jin, P. Cao and M.P. Short, GitHub data repository for this manuscript, available at https://doi.org/10.5281/zenodo.1453374.
[28] P.G. Debenedetti, F.H. Stillinger, Nature 410 (2001) 259.
[29] R.A. Vandermeer, D.J. Jensen, E. Woldt, Metall. Mater. Trans. A 28 (1997) 749–754.
[30] S.P. Hau-Riege, C.V. Thompson, Appl. Phys. Lett. 76 (2000) 309–311.
[31] K. Hattar, D. Follstaedt, J. Knapp, I. Robertson, Acta Mater. 56 (2008) 794–801.